Pergamon

Int. J. Heat Mass Transfer. Vol. 37, No. 16, pp. 2547–2559, 1994

0017-9310/94 $7.00 + 0.00

0017-9310(94)E0077-8

Double diffusive and direct instabilities below growing sea ice

M. JEROEN MOLEMAKER and HENK A. DIJKSTRA†

Institute of Marine and Atmospheric Research, Department of Physics and Astronomy, University of Utrecht, Princetonplein 5, 3584 CC Utrecht, The Netherlands

(*Received* 19 *May* 1993 *and in final form* 14 *February* 1994)

Abstract—A detailed study is presented of the instability of an initially motionless, ice-free and homogeneous layer of salt water which is sufficiently cooled from above such that ice formation occurs. Basic state boundary layer profiles of temperature and salinity are computed by solving the corresponding Stefan problem numerically. At sufficiently large Rayleigh numbers, these profiles become unstable to both direct and double diffusive instabilities. Of fundamental interest is the occurrence of a new type of oscillatory instability which is present when both temperature and salinity fields are destabilizing. Fastest growing modes are presented for the ice–water system. It is found that the wavelength of the dominant mode of convection increases with increasing ice thickness.

1. INTRODUCTION

When a homogeneous, motionless liquid layer is cooled from above, thermal instabilities (Rayleigh–Bénard) give rise to convection if a critical vertical temperature difference is exceeded [1]. In a binary liquid, for instance, with both transport of heat and salt, convection may be caused by both direct buoyancy instabilities and double diffusive instabilities. The latter instabilities occur when the stratification of the basic (motionless) state is stable. Two regimes of double diffusive instabilities are known. In the diffusive regime, heat is the destabilizing component, whereas in the finger regime salt is the destabilizing component [2].

In this paper, we consider the linear stability of a layer of salt water which is cooled from above such that freezing occurs. We are motivated by observations of large scale plumes in Arctic Seas. These plumes are thought to arise from processes at the air–sea interface [3, 4], where convection originates from an instability of temperature and/or salinity boundary layers. The salt flux is due to the formation of ice crystals if the temperature decreases below the freezing point.

The configuration of the ice–seawater system has been studied both experimentally and theoretically by, among others, Foster [5–8]. He found experimentally [7] that when the salinity is smaller than 24.7 (in the case when the freezing point temperature is smaller than the temperature of maximum density) the layer is (thermally) stable. However, as soon as ice formed, convection in the form of elongated cells developed due to the instability of the salt boundary layer. For salinities larger than 24.7, ice forms on a layer already in motion due to thermal instabilities, but the salt flux at the ice–water interface induces convection, which soon dominates the flow pattern.

Foster [6] studied the onset of the haline convection theoretically for three particular cases of the surface salt flux which defined a particular basic state salt distribution. Although he found reasonable agreement with experiments (e.g. with respect to the spatial scale of convection), the results of his stability analysis are limited because the model does not take into account the solidification of the ice and the heat transport in the ice–water system.

In this paper, a more general study of this initial development of convection is performed. In Section 2, the formulation of the problem of the cooling of an initially motionless layer of salt water from above is given. If the temperature at the air–water interface decreases below the freezing temperature, ice formation occurs. Section 3 contains results on this initial ice formation and subsequent stages by solving the governing Stefan problem. This leads to non-linear temperature and salinity profiles coupled to the ice thickness. The linear stability of these profiles is studied in Section 4 using standard numerical techniques.

From the fundamental fluid mechanics point of view, we extend work on double diffusive instabilities [9] by considering non-linear (time-dependent) basic state temperature and salinity profiles induced by cooling and solidification. The main new fundamental result is that oscillatory instabilities can occur in regions where both salt and heat are destabilizing. This instability has its origin in the different boundary layer thicknesses of temperature and salinity; the ice formation itself is only important in that it causes the formation of the different boundary layers. A description of the physical mechanism of this instability is presented in Section 5.

†Author to whom correspondence should be addressed.

NOMENCLATURE

Bi	Biot number, equation (13)
C_p	specific heat [J kg^{-1} K^{-1}]
D	diffusivity of salt [m^2 s^{-1}]
g	gravitational acceleration [m s^{-2}]
H	layer thickness [m]
h	ice thickness [m]
k	dimensionless wavenumber
L	latent heat of fusion [J K kg^{-1}]
l_x, l_z	dimensionless wavenumbers
Le	Lewis number, equation (13)
m_f	freezing point depression [K]
$\mathbf{n}$	normal to ice–water interface
p	pressure [N m^{-2}]
Pr	Prandtl number, equation (13)
Ra_T	thermal Rayleigh number, equation (13)
Ra_S	solutal Rayleigh number, equation (13)
S	salinity
S_I	constant salinity in the ice
T	temperature [°C]
T_A	temperature of ambient air [°C]
T_f	freezing temperature [°C]
$\mathbf{v}$	velocity vector [m s^{-1}]
w	vertical velocity [m s^{-1}].

Greek symbols

α	thermal expansion coefficient [K^{-1}]
β	solutal expansion coefficient
ϑ	temperature of the ice [°C]
ϑ_{int}	ice temperature at interface [°C]
κ	thermal diffusivity [m^2 s^{-1}]
λ	thermal conductivity [J m^{-1} s^{-1} K^{-1}]
μ	viscosity [kg m^{-1} s^{-1}]
ρ	density [kg m^{-3}]
σ	dimensionless complex growth factor
σ_{ia}	heat transfer coefficient [J m^{-2} s^{-1}]
σ_{wa}	heat transfer coefficient [J m^{-2} s^{-1}]
Σ	Stefan number, equation (13).

Subscripts

a	air
c	critical
i	ice
w	water
x, y, z, t	partial derivatives of x, y, z and t
∞	of the ambient fluid.

Superscripts

$'$	partial derivative of z
$\bar{}$	basic state
$\tilde{}$	perturbation.

From the laboratory point of view we find that due to ice formation vigorous convection develops instantaneously (in accordance with Foster's experiments [7]). The fastest growing mode is a direct (non-oscillatory) mode; the spatial scale of this mode increases with increasing ice thickness. The associated spatial scale is much smaller than the corresponding scale of the instability of the temperature boundary layer. Although this study is somehow related to instabilities induced by solidification (see e.g. ref. [10]) in binary liquids, we focus only on convective instabilities and do not consider interfacial tension effects (and the associated morphological instabilities).

2. FORMULATION

Consider a horizontally unbounded layer of salt water of thickness H (Fig. 1(a)). The layer is bounded below by a rigid wall and above by ambient air. The air temperature T_A far above the air–water interface is assumed to be prescribed. The liquid temperature T and salinity S far from the gas–liquid interface are constant and equal to T_∞ and S_∞, respectively. Both T and S influence the density ρ field within the water through the equation of state:

$$\rho = \rho_\infty(1+f(T,S)), \tag{1}$$

where $f(T,S)$ is a known function and $f(T_\infty, S_\infty) = 0$. With the restriction that density differences remain small with respect to the reference density ρ_∞, the Boussinesq approximation can be applied. With this approximation, the equations describing the motion within the liquid are given by

$$\nabla\cdot\mathbf{v} = 0 \tag{2a}$$

$$\rho_\infty(\mathbf{v}_t + \mathbf{v}\cdot\nabla\mathbf{v}) = -\nabla p - g\mathbf{e}_3\rho_\infty(1+f(T,S)) + \mu\nabla^2\mathbf{v} \tag{2b}$$

$$T_t + \mathbf{v}\cdot\nabla T = \kappa_w\nabla^2 T \tag{2c}$$

$$S_t + \mathbf{v}\cdot\nabla S = D\nabla^2 S. \tag{2d}$$

In these equations, $\kappa_w = \lambda_w/(\rho_\infty C_{pw})$ is the thermal diffusivity of water (where C_{pw} is the heat capacity and λ_w the thermal conductivity), μ the dynamic viscosity and D the molecular diffusivity of salt in water. All these properties are assumed to be constant. Furthermore, $\mathbf{v} = (u, v, w)^T$ is the velocity vector, p is the pressure and g is the acceleration due to gravity ($\mathbf{e}_3$ is the unit vector in the z-direction).

Boundary conditions at the lower boundary $z = -H$ are those for a no-slip wall for which the salinity and temperature are constant. Hence,

$$z = -H: \quad \mathbf{v} = 0, T = T_\infty, S = S_\infty. \tag{3a}$$

At the upper (planar) air–water interface, the interface is stress free, impervious and the heat flux over the interface is proportional to the temperature difference

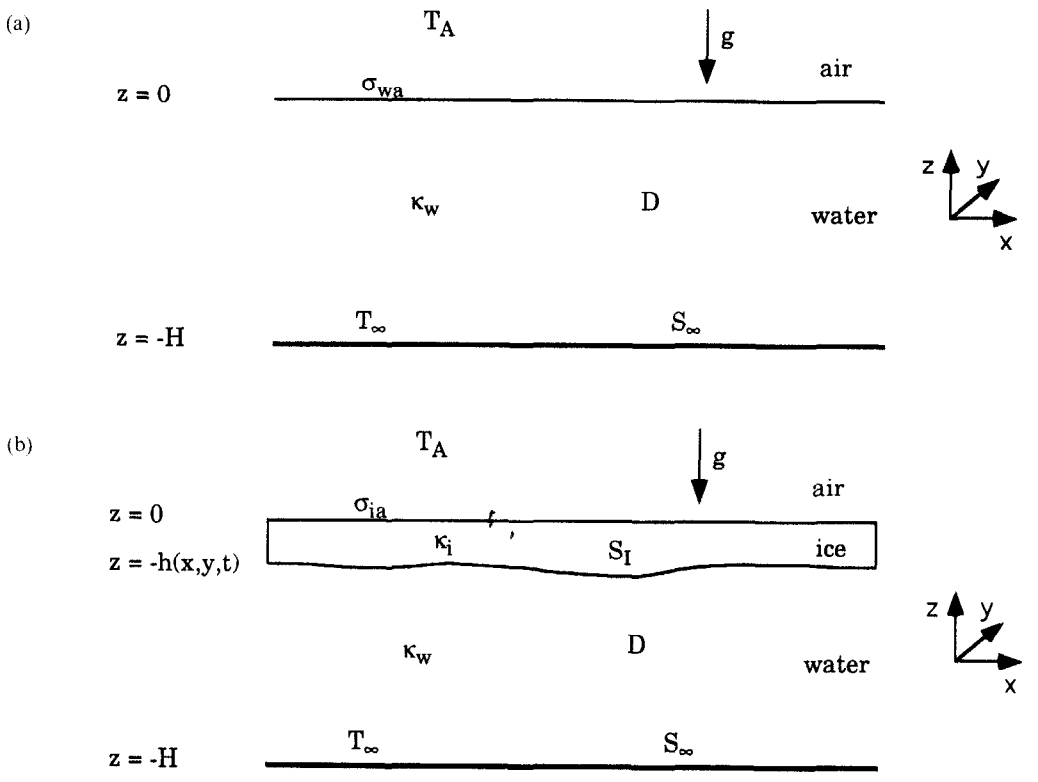

FIG. 1. Geometrical set-up of the ice-free system (a) and the ice–water system (b).

between the interface and the air temperature T_A. Hence,

$$z = 0: \quad u_z = v_z = w = 0,$$
$$-\lambda_w T_z = \sigma_{wa}(T - T_A), \quad S_z = 0, \tag{3b}$$

where σ_{wa} is an interfacial heat transfer coefficient.

If T_A is smaller than the freezing temperature of water (at salinity S_∞), ice formation occurs; let the ice–water interface be located at $z = -h(x, y, t)$ (Fig. 1(b)). When an ice layer of finite thickness is present, the boundary conditions (3b) are no longer valid. Together with the diffusion of heat in the ice which determines the ice temperature ϑ, i.e.

$$\vartheta_t = \kappa_i \nabla^2 \vartheta, \tag{4}$$

where κ_i ($\kappa_i = \lambda_i/(\rho_i C_{pi})$) is the thermal diffusivity of ice, other boundary conditions are necessary to describe the evolution of the system. At the ice–water boundary, $z = -h(x, y, t)$, these equations are (see e.g. ref. [10])

$$\rho_\infty \mathbf{v} \cdot \mathbf{n} = (\rho_\infty - \rho_i) N^{-1} h_t \tag{5a}$$
$$\mathbf{v} \cdot \mathbf{t}_1 = \mathbf{v} \cdot \mathbf{t}_2 = 0 \tag{5b}$$
$$T = \vartheta = -m_f S \tag{5c}$$
$$\mathbf{n} \cdot (-\lambda_i \nabla \vartheta + \lambda_w \nabla T) = \rho_i L N^{-1} h_t \tag{5d}$$
$$\rho_\infty D \mathbf{n} \cdot \nabla S = \rho_i h_t N^{-1} (S - S_I) \tag{5e}$$

where $\mathbf{t}_1$, $\mathbf{t}_2$ are both tangents and $\mathbf{n}$ is the (normalized) normal to the ice–water interface given by

$$\mathbf{t}_1 = (1, 0, h_x), \mathbf{t}_2 = (0, 1, h_y), \mathbf{n} = N^{-1}(-h_x, -h_y, 1). \tag{5f}$$

Furthermore, $N = (1 + h_x^2 + h_y^2)^{1/2}$ and S_I is the constant salinity in the ice, which we will take to be zero; diffusion of salt in the ice is neglected. At the ice–air interface, the heat flux is again proportional to the difference (with interfacial heat transfer coefficient σ_{ia}) between the ice temperature at the interface and the air temperature T_A. This gives

$$z = 0: \quad -\lambda_i \vartheta_z = \sigma_{ia}(\vartheta - T_A). \tag{5g}$$

Equation (5a) expresses the conservation of mass, ρ_i being the constant density of the ice. Equations (5b) express no-slip conditions, equations (5c) model continuity of temperature at the interface and the freezing point depression ($m_f > 0$) and the equations (5d) and (5e) are the heat and salt balances at the interface, respectively; L is the latent heat of fusion of ice per unit mass.

Together with given initial conditions, the evolution of the system is described for ice-free conditions by the equations (1), (2) and (3) and when ice is present by the equations (1), (2), (3a), (4) and (5).

3. PLANAR ICE GROWTH IN A MOTIONLESS LIQUID

3.1. *Formulation*

If, initially, the liquid is ice-free and motionless, there is only diffusion of heat and salt. Moreover, if

both the initial conditions and the boundary conditions for temperature and salinity are independent of x and y, these fields will only be functions of z and t. For $\mathbf{v} = 0$, equations (1)–(3) reduce to

$$p_z = -\rho_\infty g(1+f(T,S)) \tag{6a}$$

$$T_t = \kappa_w T_{zz} \tag{6b}$$

$$S_t = DS_{zz}, \tag{6c}$$

with boundary conditions

$$z = 0: \quad -\lambda_w T_z = \sigma_{wa}(T-T_A), S_z = 0 \tag{6d}$$

$$z = -H: \quad T = T_\infty, S = S_\infty. \tag{6e}$$

For general initial conditions

$$t = 0: \quad T = T_w(z), S = S_w(z) \tag{6f}$$

these equations have to be solved numerically. However, in some special cases, in particular if $H \to \infty$, $T_w(z) = T_\infty$, $S_w(z) = S_\infty$, a similarity solution of the equations (6) exists (cf. ref. [11], p. 71ff).

If $T_A < -m_f S_\infty < T_\infty$ the temperature at the air–water interface will at some time, the freezing time t_f, reach the equilibrium freezing point $T_f = -m_f S_\infty$. This freezing time t_f increases with increasing salinity S_∞ because in that case the freezing temperature decreases. The microphysical processes active to establish a thin layer of ice in a time interval $[t_f, t_f+\Delta t]$ are (at least) complicated. However, because we are interested in the change in temperature and salinity field due to a developing ice layer, a model which describes the initial growth is necessary. As undercooling phenomena and the associated non-planar growth are outside the scope of this paper, only planar ice growth in a motionless liquid is considered.

Initially, the thickness of the ice layer will be very small and therefore the associated Fourier number ($Fo = \kappa_i t/h^2$) will be large. The temperature profile in the ice can therefore be approximated as

$$\vartheta(z,t) = A(t)+B(t)z. \tag{7a}$$

The coefficients $A(t)$ and $B(t)$ can be expressed as functions of the temperature of the ice–water interface (T_f) through the boundary conditions (5g) and the first of (5c). The result is

$$A(t) = \frac{h(t)\sigma_{ia}T_A + \lambda_i T_f}{\lambda_i + h(t)\sigma_{ia}} \tag{7b}$$

$$B(t) = -\frac{\sigma_{ia}(T_f - T_A)}{\lambda_i + h(t)\sigma_{ia}}. \tag{7c}$$

If we substitute equations (7) into the boundary condition (5d) and approximate $\rho_i \cong \rho_\infty$, the equations determining the temperature and salinity fields within the liquid are given by (6b), (6c), (6e) and three other boundary conditions at the ice–water interface $z = -h(t)$, which become

$$T = -m_f S \tag{8a}$$

$$\frac{\lambda_i \sigma_{ia}}{\lambda_i + \sigma_{ia} h}(T - T_A) + \lambda_w T_z = \rho_\infty L h_t \tag{8b}$$

$$DS_z = h_t S. \tag{8c}$$

Mathematically, two of these boundary conditions serve to determine the salinity and temperature field, while a third boundary condition is necessary to solve for the unknown ice thickness $h(t)$.

At a later stage of ice formation, when the ice thickness is not small (but the liquid still remains motionless), the full problem defined by equations (4), (6b), (6c), (6e), (5c), (5d), (5e) and (5g) must be solved. For this full problem a similarity solution also exists in a semi-infinite layer approximation ($H \to \infty$) and $\sigma_{ia} \to \infty$ (which implies $\vartheta = T_A$ at the air–ice interface). Following ref. [12], where a slightly different situation is treated, these solutions are given by

$$\vartheta(z,t) = T_A - \alpha_1 Erf\left(-\frac{z}{2}(\kappa_i t)^{-1/2}\right) \tag{9a}$$

$$T(z,t) = T_\infty - \alpha_2 Erfc\left(-\frac{z}{2}(\kappa_w t)^{-1/2}\right) \tag{9b}$$

$$S(z,t) = S_\infty - \alpha_3 Erfc\left(-\frac{z}{2}(Dt)^{-1/2}\right) \tag{9c}$$

$$h(t) = 2\alpha_4 t^{1/2}, \tag{9d}$$

where the constants $\alpha_1, \ldots, \alpha_4$ (shown in the Appendix) are determined from the four boundary conditions (5c), (5d) and (5e). Characteristic for this solution is a constant salinity ($S_\infty - \alpha_3 Erfc(\alpha_4/D^{1/2})$) at the ice–water interface and developing thermal and solutal boundary layers with length scales $(\pi\kappa_w t)^{1/2}$ and $(\pi D t)^{1/2}$, respectively. As can also be seen from expressions (9), the similarity solution requires some very special initial conditions at $t = 0$. It is therefore not possible to couple this solution to an arbitrary temperature and salinity profile before freezing starts.

A basic technique to calculate the time-dependent basic state for general initial conditions is the Crank–Nicolson method using central (spatial) differences. This method is second order accurate in time and space. From $t = 0$ up to the freezing time t_f, the equations are linear and easily solved. During the initial stages of ice formation (where the ice temperature is linear in z), a new independent variable $\phi = z + h(t)$ is introduced. This coordinate transformation transforms the problem into one for a time-independent boundary. At the bottom of the liquid layer $z = -H$, the temperature and salinity fields remain constant in time. The transformed equations are non-linear and the non-linear system of algebraic equations emerging after discretization is solved by the Newton–Raphson method. Finally, when the full problem has to be solved during later stages of ice formation, a Landau transformation $\phi = -z/h(t)$ is applied to transform the numerical problem into one for a time-independent boundary.

We determined the necessary spatial and temporal numerical resolution to obtain sufficiently accurate numerical results by comparing computed fields with

the analytical solution (9) for the specific case $T_A = -3°C$, $T_\infty = 1°C$, $S_\infty = 10$. A time step $dt = 1$ s and a spatial resolution $dz = 0.75$ mm give a four digit accuracy. This resolution is used in the computations below.

3.2. *Results*

Results are shown for $T_A = -10°C$, $T_\infty = 1°C$, $S_\infty = 10$ and initial conditions $T_w(z) = T_\infty$, $S_w(z) = S_\infty$. The other parameters have values as given in the Appendix. Up to the freezing time t_f, the salinity remains constant and the temperature profile is easily solved numerically: this is the similarity solution shown in ref. [11]. The temperature distribution for three times t (in seconds) is shown in Fig. 2(a). At $t = t_f = 27.5$ s, the air–water temperature reaches the freezing temperature ($T_f = -0.53°C$) and ice formation starts.

At the transition we switch to the system of equations (7) (with $\sigma_{ia} = \sigma_{wa}$) describing the initial ice growth. Although the numerical method to compute the initial stages of ice growth is salt and heat conserving, the finite resolution introduces an error which is maximal at the transition from no ice to ice. By integrating the equations over the layer, the total salt and heat content was computed. The residues in the total salt and heat balance (both deficits) relative to the instantaneous heat and salt fluxes at the ice–water interface are no larger than 8% for this resolution, which is acceptable.

Temperature and salinity profiles are shown in Figs. 2(b–d) for three different ice thicknesses (or different times $t > t_f$). These clearly show that salt accumulates at the ice–water interface due to ice growth (advection of salt) and slow molecular diffusion. The relative increase of the amplitude of the salinity in the boundary layer is largest during the initial stages of ice growth, when the interface propagation velocity is large.

For other initial salinities (only $S_\infty = 0$ and $S_\infty = 35$ are taken), the development of the ice–water interface is qualitatively similar. In Fig. 3 the propagation speed of the ice–water interface (h_t) is shown as a function of ice thickness h for the three different initial salinities. In each case, $h_t = 0$ at $h = 0$ ($t = t_f$). This is due to the assumption that $\sigma_{wa} = \sigma_{ia}$, which implies that at $t = t_f$ the heat flux is continuous at the ice–water interface. For times $t > t_f$, initially the propagation speed increases because the heat flux from the water (at the interface) is smaller than that through the ice. However, as time progresses the freezing temperature decreases because salt is accumulating at the interface. In addition, when the ice thickness increases, the temperature at the ice–air interface decreases because heat is supplied from below less efficiently. Both effects decrease the heat flux through the ice and thereby the propagation speed. In fresh water ($S_\infty = 0$), the latter effect is the only cause of the decrease in propagation speed.

The thicknesses of both the salt boundary layer and

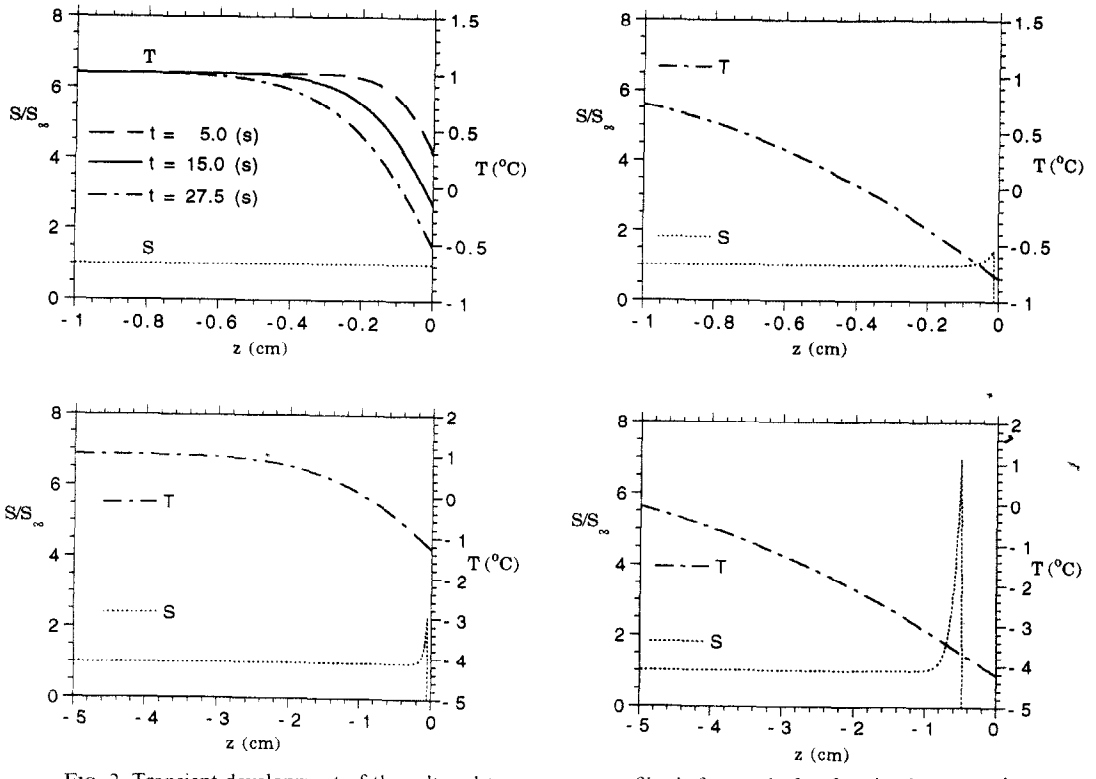

FIG. 2. Transient development of the salt and temperature profiles before and after freezing has started; $S_\infty = 10$, $T_\infty = 1°C$, $T_A = -10°C$. (a) Before freezing. (b) $h = 0.01$ cm. (c) $h = 0.05$ cm. (d) h = 0.5 cm.

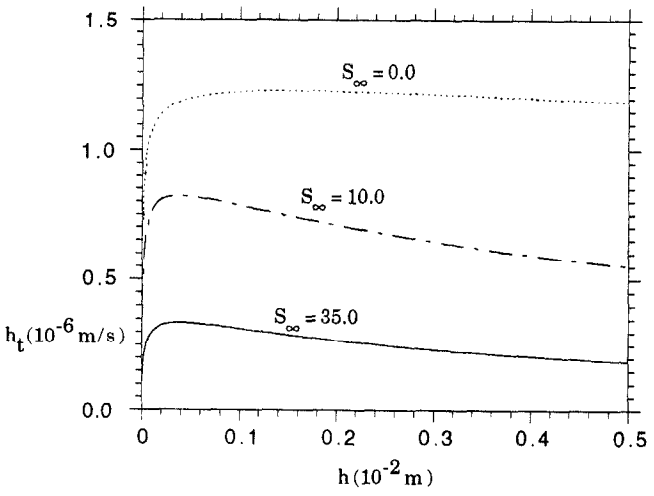

FIG. 3. Growth rate of the interface as a function of h for three different salinities: $S_\infty = 0$, 10 and 35.

the temperature boundary layer increase with $S_\infty > 0$ (at the same ice thickness). The salt concentration (relative to S_∞) at the ice–water interface decreases with increasing S_∞. Both results are related to the fact that the growth rate of the ice layer decreases with increasing S_∞ (cf. Fig. 3). As it takes longer to reach a particular ice thickness for larger S_∞, the penetration depths of both (temperature and salinity) boundary layers are larger. More salt has been transported by diffusion and the interface concentration (relative to S_∞) is therefore smaller.

4. LINEAR STABILITY PROBLEM

4.1. *Formulation*

Suppose that a temperature and salinity field $\bar{T}(z,t)$, $\bar{S}(z,t)$ and ice thickness $\bar{h}(t)$ have been calculated numerically up to a certain time t^*. Since the temperature near the ice–water boundary will decrease and the salinity will increase, the density may increase at the top of the water layer. Hence, this layer may become unstable to both double diffusive and direct buoyancy instabilities, depending on the the explicit form of the equation of state (1).

To determine sufficient conditions for instability, a standard linear stability analysis is performed. Each dependent variable is expressed as the sum of the basic state and some arbitrary disturbance (denoted by a tilde):

$$\{\mathbf{v}, \vartheta, T, S, p\}(x,y,z,t) = \{\mathbf{0}, \bar{\vartheta}, \bar{T}, \bar{S}, \bar{p}\}(z,t) + \{\tilde{\mathbf{v}}, \tilde{\vartheta}, \tilde{T}, \tilde{S}, \tilde{p}\}(x,y,z,t) \quad (10a)$$

$$h(x,y,t) = \bar{h}(t) + \tilde{h}(x,y,t). \quad (10b)$$

Linearization in the primed quantities and nondimensionalizing the emerging equations by scales H, H^2/κ_w, κ_w/H, $\mu\kappa_w/H^2$, T_∞ and S_∞ for length, time, velocity, pressure, temperature and salinity, respectively, leads eventually to the evolution equations for infinitesimally small disturbances.

In a quasi-steady state approximation the basic state is 'frozen' at some time t^*. It can be shown that growth factors computed with this approximation are only valid for small times $\tau = t - t^*$ [13, 14]. The actual time interval of validity depends on the ratio of the time rate of change of the basic state and perturbations (the growth factors) and the approximation of the instantaneous growth factors becomes better if this ratio decreases (large growth factors).

In this approximation, a normal mode approach is followed, i.e. the linearized equations admit solutions of the form

$$\{\tilde{\mathbf{v}}, \tilde{\vartheta}, \tilde{T}, \tilde{S}, \tilde{p}\}(x,y,z,t) = \{\hat{\mathbf{v}}, \hat{\vartheta}, \hat{T}, \hat{S}, \hat{p}\}(z) \times \exp(i(l_x x + l_y y) + \sigma t) \quad (11a)$$

$$\tilde{h}(x,y,t) = \hat{h} \exp(i(l_x x + l_y y) + \sigma t). \quad (11b)$$

Here σ is the complex growth factor and l_x, l_y are horizontal wavenumbers. If $\mathscr{R}(\sigma) > 0$ then the perturbations will grow and the basic state is unstable.

Elimination of the pressure and horizontal velocities finally leads to the following two-point boundary eigenvalue problem (where the primes indicate differentiation to z and $k^2 = l_x^2 + l_y^2$). On $z \in (-\bar{h}, 0)$:

$$\vartheta'' - \vartheta\left(\frac{\sigma}{\kappa} + k^2\right) = 0; \quad (12a)$$

On $z \in (-1, -\bar{h})$:

$$w'''' - w''(\sigma Pr^{-1} + 2k^2) + w(k^4 + \sigma Pr^{-1} k^2) = k^2(Ra_S S + Ra_T T) \quad (12b)$$

$$S'' - S(\sigma Le + k^2) = Lew\bar{S}_z \quad (12c)$$

$$T'' - T(\sigma + k^2) = w\bar{T}_z \quad (12d)$$

with boundary conditions

$$z = 0: \quad \vartheta' = -Bi\,\vartheta \quad (12e)$$

$$z = -\bar{h}: \quad \vartheta = T - h(\bar{T}_z - \bar{\vartheta}_z) = mS - h(m\bar{S}_z - \bar{\vartheta}_z) \quad (12f)$$

$$w = w' = 0 \tag{12g}$$

$$Le^{-1}S' - \bar{h}_t S = h(Le^{-1}\bar{S}_{zz} + \sigma\bar{S} - \bar{h}_t\bar{S}_z) \tag{12h}$$

$$\Sigma\sigma h = -\lambda\vartheta' + T' + h(\lambda\bar{\vartheta}_{zz} - \bar{T}_{zz}) \tag{12i}$$

$$z = -1: \quad w = w' = T = S = 0. \tag{12j}$$

In these equations several dimensionless parameters appear. These are the thermal Rayleigh number Ra_T, the solutal Rayleigh number Ra_S, the Prandtl number Pr, the Lewis number Le, the Biot number Bi, the ratio of thermal conductivities of ice and water λ, the ratio of thermal diffusivities κ, the Stefan number Σ and the freezing point depression coefficient m. These parameters are defined as

$$Ra_T = \rho_\infty \frac{gH^3\alpha}{\mu\kappa_w} T_\infty \quad Ra_S = \rho_\infty \frac{gH^3\beta}{\mu\kappa_w} S_\infty$$

$$Pr = \frac{\mu}{\rho_\infty \kappa_w}$$

$$Le = \frac{\kappa_w}{D} \quad m = m_f \frac{S_\infty}{T_\infty} \quad \Sigma = \frac{L}{C_{pw} T_\infty}$$

$$\lambda = \lambda_i/\lambda_w \quad \kappa = \kappa_i/\kappa_w \quad Bi = \sigma_{ia} H/\lambda_i \tag{13}$$

where $\alpha = (\partial f/\partial T)|_{\bar{T},\bar{S}}$ and $\beta = (\partial f/\partial S)|_{\bar{T},\bar{S}}$. Note that these coefficients α and β depend on the vertical coordinate through the basic state profiles. The temperature perturbation in the ice can be solved explicitly (using (12a) and (12e)) to give

$$\vartheta(z) = \vartheta_{int} \frac{(Bi+q)e^{-qh} - (Bi-q)e^{qh}}{(Bi+q)e^{qh} - (Bi-q)e^{-qh}}, \tag{14}$$

where ϑ_{int} is the perturbation ice temperature at the ice–water interface and $q^2 = k^2 + \sigma^2/\kappa$. Now ϑ_{int} can be expressed into the other dependent variables through the first equation of (12f). Thereafter, the expression (14) can be used to eleminate ϑ from the boundary condition (12i). This finally leads to an eigenvalue problem for the eigenvector $(w, h, T, S)^T$.

The two-point boundary eigenvalue problem (12) was solved by standard continuation software for ODEs, the AUTO [15] package. The system of equations (12) is written as a system of first order autonomous equations and treated as a bifurcation problem. Eigenvalue curves (which are non-trivial solutions of these equations) can be easily detected and branches of eigenvalues can be traced through parameter space. When λ denotes any free parameter and $\mathbf{u}$ is the solution vector, the accuracy of AUTO was set at $|\lambda|/(1+|\lambda|) < 10^{-6}$ and $|\mathbf{u}|/(1+|\mathbf{u}|) < 10^{-6}$. Eigenvalue curves for a linear temperature and salinity profile compared favourably with those computed analytically by Baines and Gill [9].

4.2. *Results*

In the linear stability analysis of the basic states, computed in the previous section, the time t^* (at which these basic states are 'frozen') is treated as an additional parameter. We will only consider the case for which α and β (and thereby Ra_T and Ra_S) are constant. Other parameters are fixed and their values are given in the Appendix. Stability boundaries are shown for several 'reduced' problems by 'deforming' the basic states from those for linear temperature and salt profiles to those below growing sea-ice. This is done to clarify the relation between the unstable modes for these basic states and those considered by Baines and Gill [9].

For the most simple case $\vartheta = h = 0$ ((12g,h) are dropped) and constant $\bar{S}_z > 0$, $\bar{T}_z < 0$, we recover the case in ref. [9] but with a rigid top and bottom wall. For a fixed value of Ra_S, there are an infinite number of eigenvalues Ra_T satisfying the eigenvalue problem at neutral stability [2]. The eigenfunctions of these modes can be distinguished by the number of zeroes in the vertical velocity. For $Ra_S = 0$, these are stationary instabilities (the first eigenvalue being the classical Rayleigh–Bénard value $Ra_T = 1708$). In Fig. 4(a), stability boundaries are shown for the first two modes in the Ra_S–Ra_T plane. Solid lines correspond to stationary modes, dotted lines to oscillatory modes (each point corresponds to a minimum of a neutral curve). A positive value of Ra_T corresponds to a destabilizing thermal field and a negative Ra_S corresponds to a destabilizing salt field. Plots of the eigenfunctions at several marked points in Fig. 4(a) are shown in Fig. 5 for further reference. In these figures, $\rho(T) = Ra_T T(z)$ and $\rho(S) = Ra_S S(z)$ are plotted

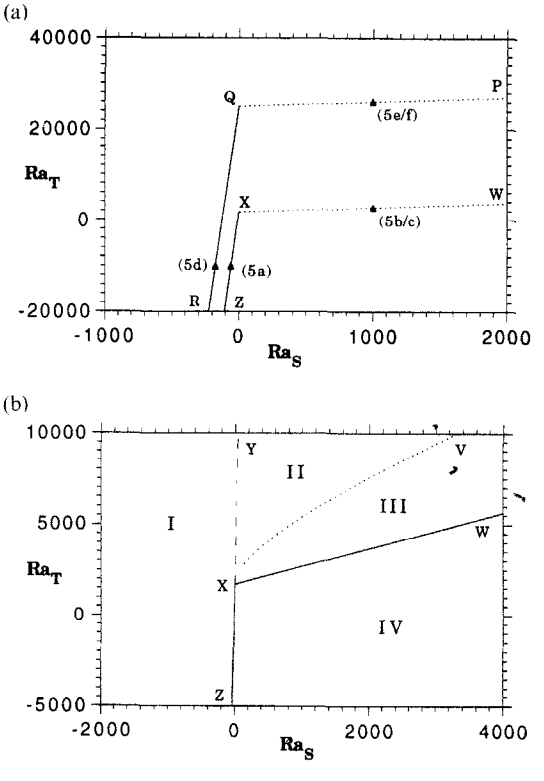

FIG. 4. Stability boundaries for the basic state with constant $\bar{T}_z < 0$ and constant $\bar{S}_z > 0$. (a) Stability boundaries of both first and second modes. (b) Details of only the first mode.

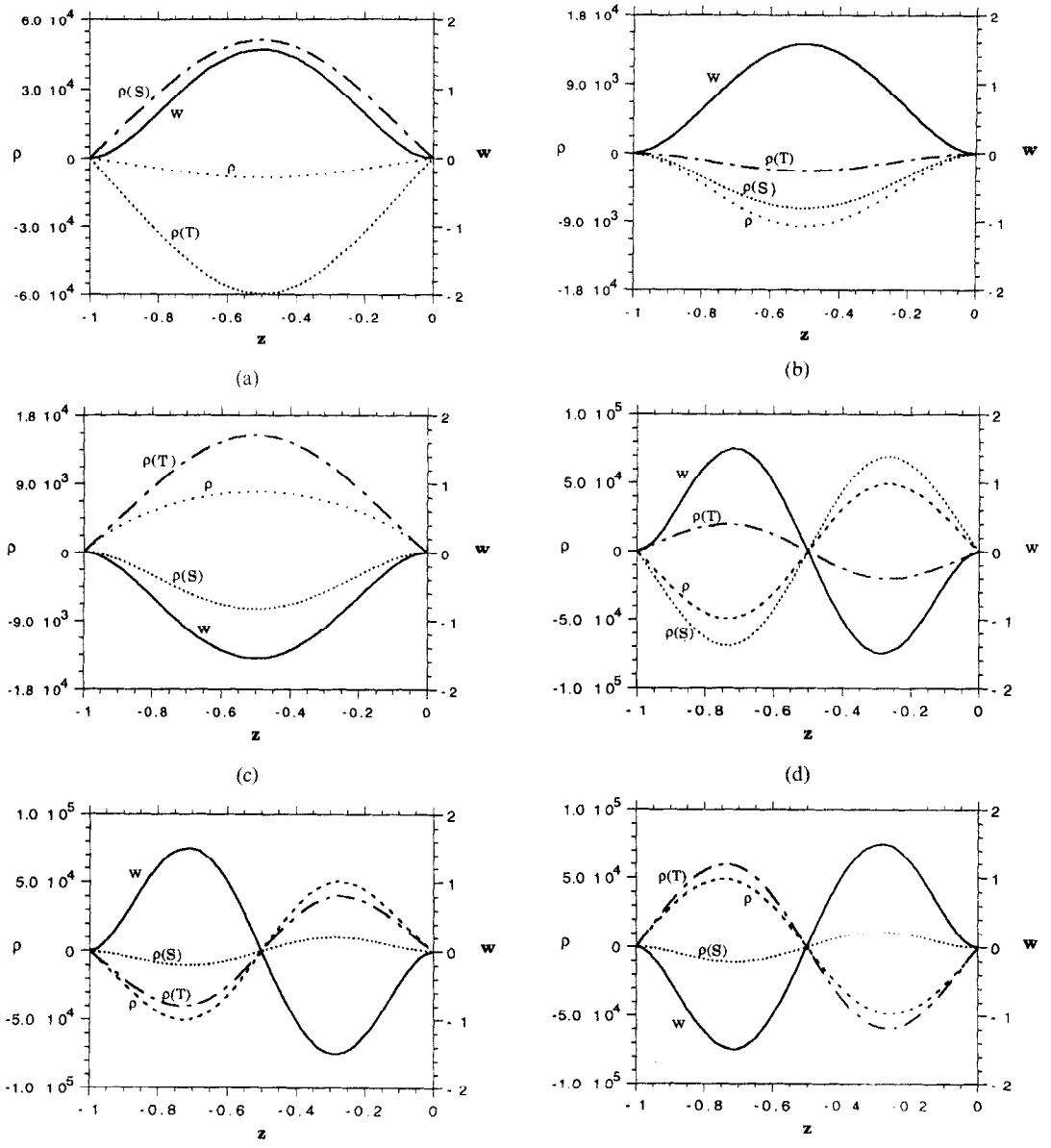

FIG. 5. Eigenfunctions at labelled points in Fig. 4(a). $\rho(S) = Ra_S S$, $\rho(T) = Ra_T T$, $\rho = \rho(T) + \rho(S)$ and w is the perturbation vertical velocity. (a) First vertical mode (dir.), $Ra_T = -10^4$, $Ra_S = -58.5$. (b) First vertical mode (osc./Re), $Ra_T = 2700$, $Ra_S = 1000$. (c) First vertical mode (osc./Im), $Ra_T = 2700$, $Ra_S = 1000$. (d) Second vertical mode (dir.), $Ra_T = -10^4$, $Ra_S = -174$. (e) Second vertical mode (osc./Re), $Ra_T = 2.6 \times 10^4$, $Ra_S = 1000$. (f) Second vertical mode (osc./Im), $Ra_T = 2.6 \times 10^4$, $Ra_S = 1000$.

(instead of $T(z)$ and $S(z)$) to show each contribution to the density perturbation in the liquid. Also plotted are the total density perturbation ρ and the vertical velocity perturbation w. For oscillatory modes, both real and imaginary parts of the eigenfunctions are presented. The first modes for which the vertical velocity has no zeroes (Figs. 5(a–c)) are more unstable than the second modes, which have one zero (Figs. 5(d–f)).

In Fig. 4(b), more detailed stability boundaries for the first modes are given by drawn lines. In this figure, dashed lines mark changes in the number of unstable modes. There is only one unstable stationary mode in region I. In region II, there are two unstable stationary modes. In region III, an oscillating mode (travelling waves in both horizontal directions) is unstable. At the line X–V in the diagram, the frequency of these travelling waves tends to zero. In the eigenvalue plane, a bifurcation occurs and two stationary branches appear (corresponding to the two stationary unstable modes in region II). For one of these modes, the growth factor decreases and this mode becomes neutral on the curve X–Y. The other mode remains unstable as X–Y is crossed.

The critical wavenumber k_c along the curve Z–X–

W is constant ($k_c = 3.12$) and is larger than the value found for 'slippery' top and bottom walls ($k_c = 2.22$ [9]). This difference is well known from the single component Rayleigh–Bénard instability [2]. If Ra_S (with fixed Ra_T) is decreased (more negative) from a point on the curve X–Z, k_c increases whereas the eigensolution still extends over the whole liquid layer. This implies that the most unstable modes are long and narrow, which characterizes 'salt fingers'.

To study the influence of the (basic state) temperature and salinity boundary layer profiles, we consider next the case $\vartheta = h = 0$, but $\bar{T}_z$ and $\bar{S}_z$ are now profiles calculated below the growing ice. The stability boundaries for the temperature and salinity field shown in Fig. 2(c) (ice thickness 0.5 mm) are presented in Fig. 6. The stability boundary Z–W in Fig. 6 is the modified stability boundary Z–W in Fig. 4(a). Critical Rayleigh numbers have increased showing that the mode is more stable. The second vertical mode (branch R–Q–P in Fig. 4(a)) has changed into an oscillatory branch R–U, now occurring for negative Ra_S, and a stationary branch U–V. In addition, a third oscillatory branch Q–P appears.

Again, eigensolutions are plotted in Fig. 7(a–f) at selected (labelled) points in Fig. 6. The critical wavenumber k_c is not constant along the branch X–Z (as it is in Fig. 4(a)), but increases with increasing $|Ra_T|$. This can be seen by comparing Fig. 5(a) and 7(d). In the latter figure, the disturbances are more confined to the boundary layer, indicating a smaller spatial scale (i.e. larger k_c). Along the branch X–W, the critical wavenumber is nearly constant ($k \cong 3.5$). For this mode, the vertical velocity and temperature perturbations extend over the whole layer, whereas the salinity perturbation is confined to the boundary layer (compare Figs. 7(c/f) with 5(b/c).

It is interesting that oscillatory instabilities (R–U) are present in an area where both salt and temperature are destabilizing. The mechanism of this instability and its relevance for the ice–water system is discussed below. Along the branch R–U, the wavenumber is nearly constant ($k \cong 6.0$). At very large negative Ra_S

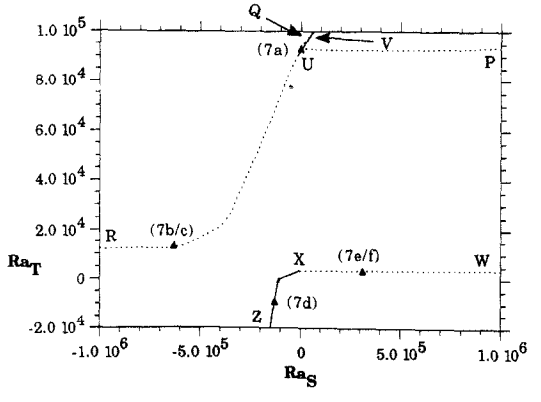

FIG. 6. Stability boundaries for salt and temperature boundary layer profiles at $\bar{h} = 0.05$ cm, but with the restriction that all perturbation quantities vanish at the ice–water interface.

another direct mode (not shown in Fig. 6) becomes unstable. Other eigenmodes (branches U–V and Q–P in Fig. 6) can be interpreted as mixed modes or 'boundary layer modified' modes. Since these modes are irrelevant for the ice–water system ($Ra_S < 0$) we do not discuss them further.

Next, the stability problem for the full ice–water model (equations (12)) is considered. Results for the stability boundaries for $\bar{h} = 0.05$ cm are shown in Fig. 8. The results in Fig. 6 are only slightly modified. The stability has decreased due to the additional freedom of interface perturbations. No new instabilities are found. With respect to the eigenfunctions (not shown), the main difference is the disappearance of the steep gradients in salinity and temperature perturbations near the ice–water interface. Otherwise, the eigenfunction structures resemble those in Fig. 7.

5. DISCUSSION

In this paper, the onset of convection due to double diffusive and direct instabilities below growing sea-ice is considered. The basic state temperature and salinity profiles below the ice are calculated by solving the appropriate Stefan problem for planar ice growth.

Using the quasi-steady approximation and constant (Ra_T, Ra_S), stability boundaries are calculated. A new oscillatory instability is found in the region $Ra_T > 0$, $Ra_S < 0$ where both the basic state salt and temperature distribution are destabilizing. A description of the mechanism of this instability is attempted with the help of Fig. 9. Here, the spatial structures of the perturbations, corresponding to the eigenfunctions of Figs. 7(b) and (c), are shown over half an oscillation period. In Fig. 9(a) (start of the description), there is a small region 1 (indicated in Fig. 9(a)) where the vertical velocity perturbation is slightly negative. Fluid elements in this region are saltier than their environment and move downward. In region 2 (also indicated in Fig. 9(a)), fluid elements are lighter (warmer) than their environment and move upward (the salt perturbation is nearly zero). In region 2, advection of heat is larger than diffusion, thereby increasing the temperature perturbation and the vertical velocity (Fig. 9(b)). The region of positive vertical velocity expands upward and erodes region 1. As the velocities in region 1 reverse sign, the salt perturbation (dominated by advection) becomes negative (Fig. 9(c)). Velocities in the transition region are very small and salt diffuses downward, increasing the density at the top of region 2 (Fig. 9(d)). Thereby the velocities in region 2 decrease and eventually reverse sign (Fig. 9(e)). Due to advection of heat, the (negative) temperature perturbation increases and thereby also the (negative) vertical velocities in region 2 (Fig. 9(f)). Here, the cycle starts again with reversed sign.

We now consider the relevance of these results for the ice–seawater system. Thereby we are restricted to constant α and β, which gives a restriction on the values of (T_∞, S_∞). In Fig. 10(a), the freezing point

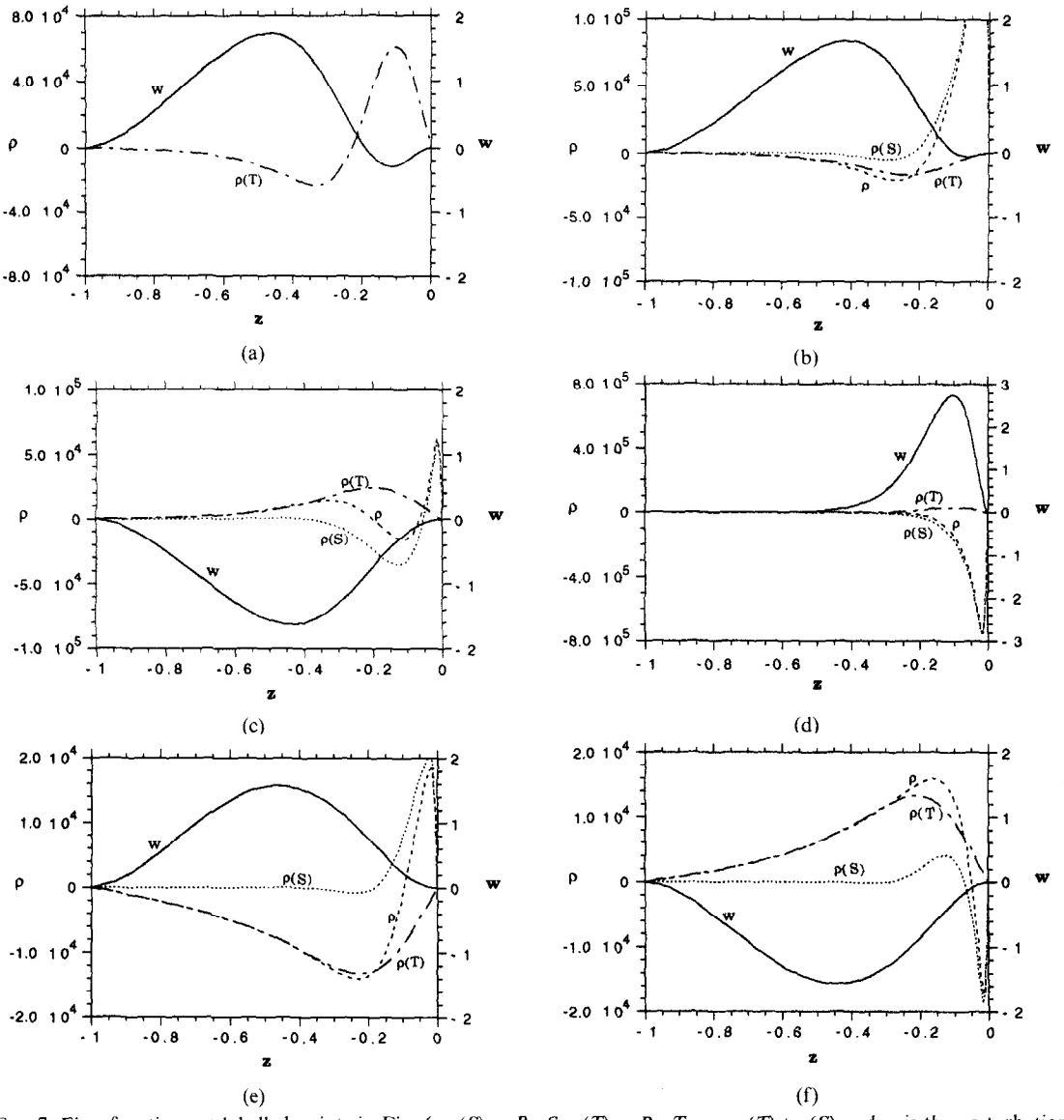

FIG. 7. Eigenfunctions at labelled points in Fig. 6. $\rho(S) = Ra_S S$, $\rho(T) = Ra_T T$, $\rho = \rho(T) + \rho(S)$ and w is the perturbation vertical velocity. (a) (dir.), $Ra_T = 9.3 \times 10^4$, $Ra_S = 0$, $k_c = 6.9$. (b) (osc./Re), $Ra_T = 1.3 \times 10^4$, $Ra_S = -6.3 \times 10^5$, $k_c = 6.1$. (c) (osc./Im), $Ra_T = 1.3 \times 10^4$, $Ra_S = -6.3 \times 10^5$, $k_c = 6.1$. (d) (dir.), $Ra_T = -8.9 \times 10^3$, $Ra_S = -1.3 \times 10^5$, $k_c = 18.0$. (e) (osc./Re), $Ra_T = 3.5 \times 10^3$, $Ra_S = 3.1 \times 10^5$, $k_c = 3.4$. (f) (osc./Im), $Ra_T = 3.5 \times 10^3$, $Ra_S = 3.1 \times 10^5$, $k_c = 3.4$.

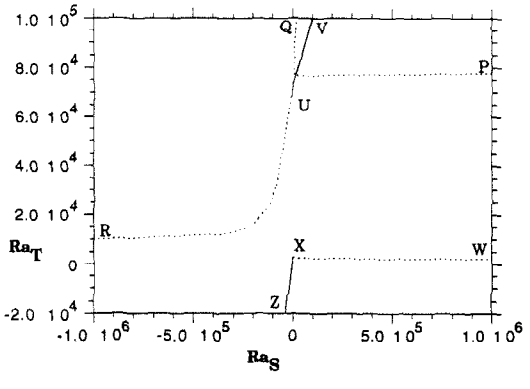

FIG. 8. Stability boundaries for the full coupled air–ice–water system and the basic state salt and temperature boundary layer profiles at $\bar{h} = 0.05$ cm.

curve and the curve of maximum density are shown in the (T, S) plane. For (T_∞, S_∞) in region I, $\alpha > 0$ and $\beta < 0$ are approximately constant and the temperature boundary layer might become unstable before any freezing occurs. This depends upon the critical Ra_T number as the temperature profile evolves before freezing; $Ra_{Tc} \cong 9.4 \times 10^3$ at $t = t_f$. For $t < t_f$ the neutral curve is shifted upwards and to the right. Hence for $Ra_T < Ra_{Tc}$, ice formation will occur in a motionless liquid. If $Ra_T > Ra_{Tc}$ the ice-free layer is unstable and the theory formally does not apply, since the ice growth is affected by convection.

For $Ra_T = 9 \times 10^3$, $Ra_S = -10^8$ and three different ice thicknesses $\bar{h}$ (associated with three different times at which the basic state is 'frozen'), growth factors of the most unstable mode are shown in Fig. 10(b) as a function of wavenumber k. Since the growth factors

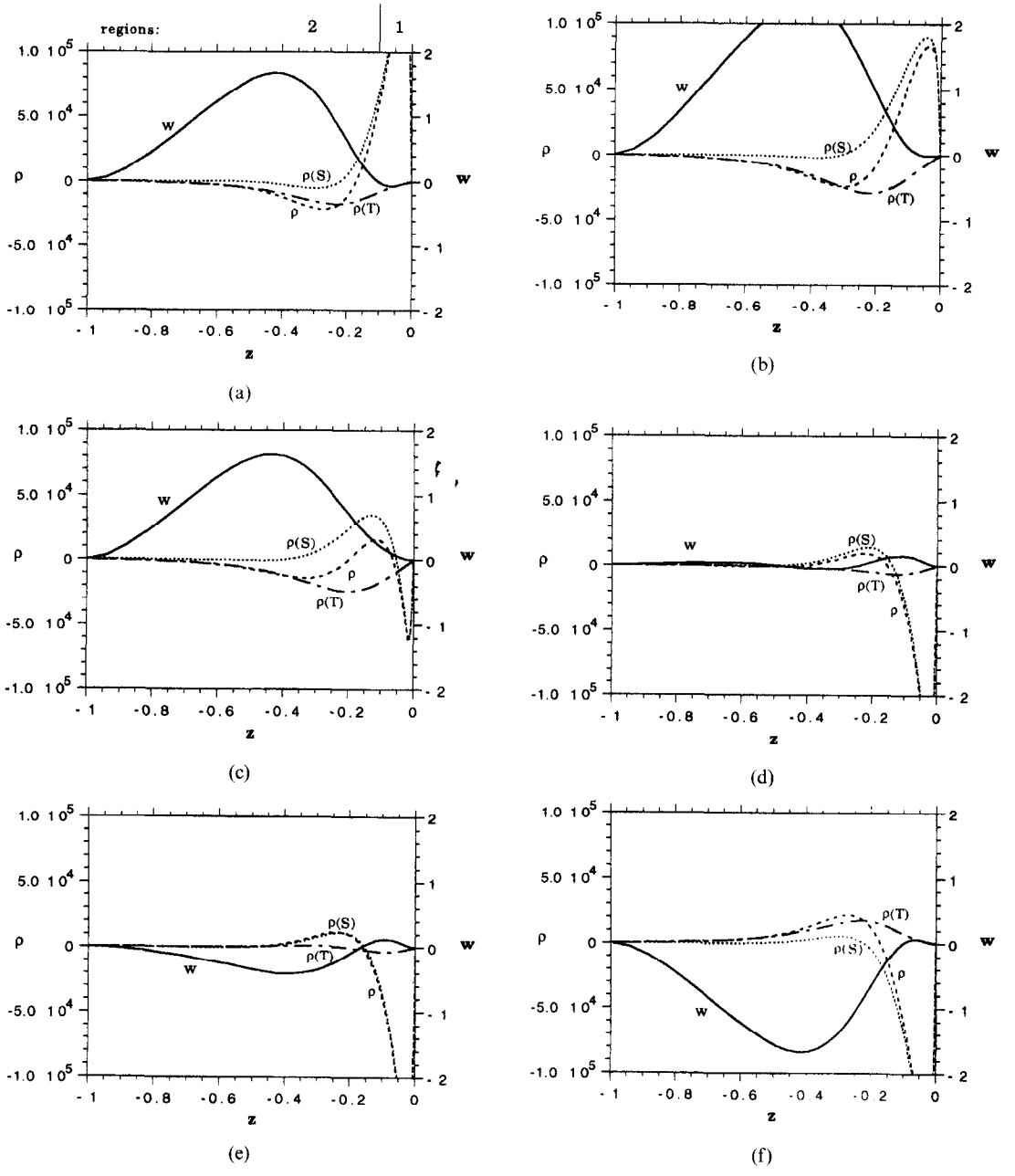

FIG. 9. Illustration of the mechanism of the mixed oscillatory mode in Figs. 7(b) and (c). The spatial structures evolving over half an oscillation period τ are presented. (a) $t/\tau = 0.000$; (b) $t/\tau = 0.125$; (c) $t/\tau = 0.250$; (d) $t/\tau \simeq 0.375$; (e) $t/\tau = 0.400$; (f) $t/\tau = 0.500$.

are very large, the quasi-steady approximation is justified. The wavenumber with maximum growth (for which perturbation structures are plotted in Fig. 10(c)) decreases with increasing ice thickness (over the range considered). The magnitude of this wavenumber and the density perturbation is mainly controlled by the buoyancy flux due to salt rejection. From Fig. 8, we observe that for $Ra_T = 9 \times 10^3$, the oscillatory mode is stable for $\bar{h} = 0.05$ cm. Although this mode becomes unstable for $\bar{h} = 0.1$ cm, the growth factors are orders of magnitude smaller than those shown in Fig. 10(b). The same is true for the direct mode, which is unstable for very large $|Ra_S|$.

For (T_∞, S_∞) in region II and for which the salt concentration at the interface remains in region II, $\alpha < 0$ and $\beta < 0$ are approximately constant. The ice-free layer is stable up to the freezing point and ice formation occurs in a motionless layer with $Ra_T < 0$ and $Ra_S < 0$. In this case, there is only one direct unstable mode. The variation with ice thickness is the same as shown for the direct mode in Fig. 10(b), because growth factors for this mode hardly depend

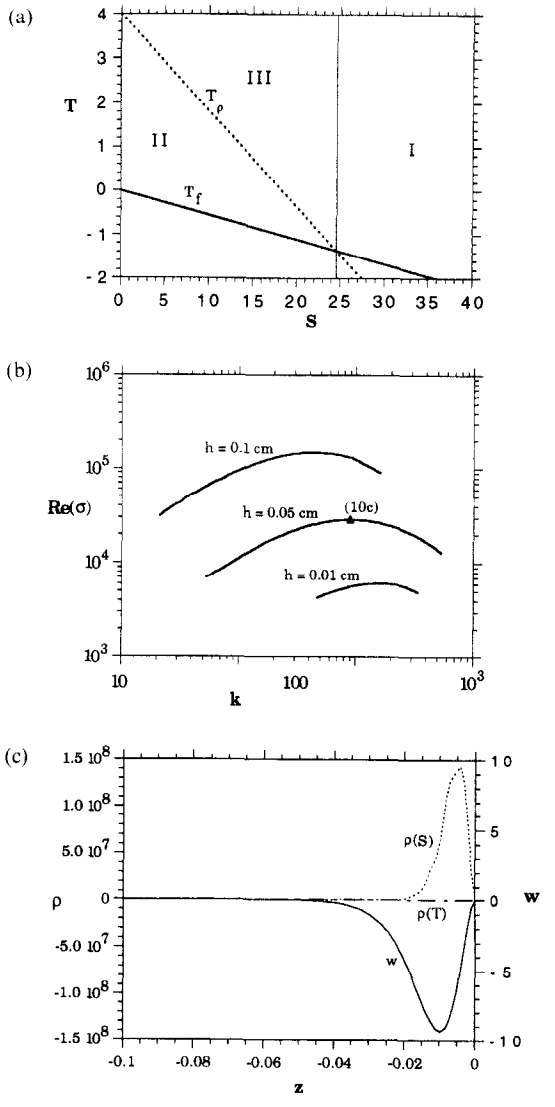

FIG. 10. (a) T–S diagram showing the curve of maximum density T_ρ and the freezing point curve T_f. (b) Growth factors of the most unstable direct mode for $Ra_S = -10^8$, $Ra_T = 9 \times 10^3$ and different ice thicknesses $\bar{h}$. (c) Eigenfunctions at $\bar{h} = 0.05$ cm at the maximum growth rate ($k = 199.5$).

on Ra_T. For example, at $\bar{h} = 0.1$ cm and $Ra_S = -10^8$, the values of maximum growth factor σ_{max} and corresponding wavenumber k_{max} are $(1.547 \times 10^4, 123.9)$ and $(1.545 \times 10^4, 125.9)$ for $Ra_T = 9.0 \times 10^3$ and $Ra_T = -10^6$, respectively.

Finally, for (T_∞, S_∞) in region III, the theory does not apply, because α is not constant over the liquid layer. In this case, the problem is more complicated due to the presence of a potentially stable layer sandwiching the ice and an unstable layer.

In physical situations where the theory is applicable (within the limits of the model), the initial development of convection is as follows. For a system with fixed Rayleigh numbers Ra_T and Ra_S, there is a certain ice thickness (reached at a certain 'onset' time t_0) up to which the basic state temperature and salinity profile below the growing ice remains stable. A certain range in wavenumbers becomes unstable for times larger than t_0. Growth factors of these unstable modes are shown in Fig. 10(b) at certain fixed times $t^* > t_0$. For times $\tau = t - t^*$ small compared to t^*, these unstable modes will grow exponentially in time. This picture is valid as long as the amplitudes of the disturbances remain small and non-linear interactions can still be neglected.

How do these results compare with experiments? As found by Foster about 25 years ago [7, 8] the onset times are very small compared to typical times in which a layer of ice of reasonable thickness (1–10 cm) is grown. Also, the associated spatial scales are small compared to the depth of the fluid layer. Since growth factors of unstable disturbances are very large at realistic Rayleigh numbers, non-linear interactions become important almost instantaneously. In typical experiments [16–18], it is shown that non-linear interactions lead to sheet-like plumes in which colder and saltier fluid moves downward in relatively narrow regions, whereas warmer fluid is upwelled over relatively larger regions (with relatively smaller velocities).

The analysis in this paper is not capable of describing the finite amplitude convection. However, the linear stability analysis provides an adequate starting point to study plume formation (on laboratory scales) at large Rayleigh numbers. It is our opinion that since this type of buoyancy convection occurs on scales of millimetres to several kilometres in nature, the study of plume formation below ice on a laboratory scale may provide inherent characteristics of this convection (i.e. in particular the dependence of spatial scales on the main driving force) which may not be easily isolated for study in larger scale systems.

Acknowledgements—All computations were performed on the CRAY Y-MP at the Academic Computing Centre (SARA), Amsterdam, the Netherlands within the project SC212. Use of these computing facilities was sponsored by the Stichting Nationale Supercomputerfaciliteiten (National Computing Facilities Foundation, NCF) with financial support from the Nederlandse Organisatie voor Wetenschappelijk Onderzoek (Netherlands Organization for Scientific Research, NWO). The authors thank Prof. Will de Ruijter (IMAU) for much encouragement and support.

REFERENCES

1. Lord Rayleigh, *Phil. Mag.* **32**, 529–549 (1916).
2. J. S. Turner, *Buoyancy Effects in Fluids*, Chap. 1. Cambridge University Press, Cambridge (1973).
3. G. C. Gascard, Open ocean convection and deep water formation revisited in the Mediterranean, Labrador, Greenland and Weddell seas. In *Deep Convection and Deep Water Formation in the Oceans* (Edited by P. C. Chu and J. C. Gascard). Elsevier, Amsterdam (1991).
4. B. Rudels, Haline convection in the Greenland Sea, *Deep Sea Res.* **37**, 1491–1511 (1990).
5. T. D. Foster, Stability of a homogeneous fluid cooled uniformly from above, *Physics Fluids* **8**, 1249–1257 (1965).

6. T. D. Foster, Haline convection induced by the freezing of sea water, *J. Geophys. Res.* **73,** 1933–1938 (1968).
7. T. D. Foster, Experiments on haline convection induced by the freezing of sea water, *J. Geophys. Res.* **74,** 6967–6974 (1969).
8. T. D. Foster, Haline convection in Polynyas and Leads, *J. Phys. Oceanogr.* **2,** 462–469 (1972).
9. P. G. Baines and A. E. Gill, On thermohaline convection with linear gradients, *J. Fluid Mech.* **37,** 289–306 (1969).
10. M. E. Glicksman, S. R. Coriell and G. B. McFadden, Interaction of flows with the crystal-melt interface, *Ann. Rev. Fluid Mech.* **18,** 307–335 (1986).
11. H. S. Carslaw and J. C. Jeager, *Conduction of Heat in Solids* (1st edn), p. 53. Clarendon Press, Oxford (1947).
12. S. Martin and P. Kauffman, An experimental and theoretical study of the turbulent and laminar convection generated under a horizontal ice sheet floating on warm salty water, *J. Phys. Oceanogr.* **7,** 272–283 (1977).
13. M. J. M. Krane and B. Gebhart, The hydrodynamic stability of a one-dimensional transient buoyancy-induced flow, *Int. J. Heat Mass Transfer* **36,** 977–988 (1993).
14. H. A. Dijkstra and A. I. Van de Vooren, Initial flow development due to Marangoni convection in a mass transfer system, *Int. J. Heat Mass Transfer* **12,** 2315–2322 (1985).
15. E. J. Doedel, AUTO : a program for the automatic bifurcation analysis of autonomous systems, *Proc. 10th Manitoba Conf. on Numerical Math. Comput.*, Vol. 30, pp. 265–274 (1980).
16. R. Farhadieh and R. S. Tankin, A study of the freezing of sea water, *J. Fluid Mech.* **71,** 293–304 (1975).
17. K. B. Katsaros, W. T. Liu, J. A. Businger and J. E. Tillman, Heat transport and thermal structure in the interfacial boundary layer measured in an open tank of water in turbulent free convection, *J. Fluid Mech.* **83,** 311–335 (1977).
18. J. A. Whitehead and M. M. Chen, Thermal instability and convection of a thin fluid layer bounded by a stably stratified region, *J. Fluid Mech.* **40,** 549–576 (1970).

APPENDIX: VALUES OF PARAMETERS AND COEFFICIENTS USED IN THE CALCULATIONS

A1. *Dimensional parameters*

$\kappa_w = 1.44 \times 10^{-7}\ m^2\ s^{-1}$ $\quad \lambda_i = 5.30 \times 10^{-1}\ J\ m^{-1}\ s^{-1}\ K^{-1}$

$\kappa_i = 1.15 \times 10^{-6}\ m^2\ s^{-1}$ $\quad \lambda_w = 1.44 \times 10^{-1}\ J\ m^{-1}\ s^{-1}\ K^{-1}$

$D = 7.00 \times 10^{-10}\ m^2\ s^{-1}$ $\quad \sigma_{oa} = \sigma_{ia} = 1.0 \times 10^{1}\ J\ m^{-2}\ s^{-1}$

$\rho_i = \rho_\infty = 1.0 \times 10^{3}\ kg\ m^{-3}$ $\quad \mu = 2.0 \times 10^{-3}\ kg\ m^{-1}\ s^{-1}$

$\rho_i L = 7.3 \times 10^{7}\ J\ K\ m^{-3}$ $\quad H = 0.10\ m.$

A2. *Values of dimensionless parameters*

$$Pr = 14 \quad Bi = 1.75 \quad Le = 200 \quad \lambda = 4$$

$$\kappa = 7 \quad m = -0.5 \quad \Sigma = 73.$$

B. *Coefficients* α_i

$$\alpha_1 = (Erf(\eta))^{-1}(T_A - m_f(S_\infty - \alpha_3 Erfc(\gamma))$$

$$\alpha_2 = (Erf(\zeta))^{-1}(T_\infty - m_f(S_\infty - \alpha_3 Erfc(\eta))$$

$$\alpha_3 = S_\infty(Erfc(\gamma) - \pi^{-1/2}\gamma^{-1}\exp(-\gamma^2))^{-1}$$

$$\alpha_4 = -L^{-1}\{(\pi\kappa_i)^{-1/2}\alpha_1\lambda_i\exp(-\eta^2) + (\pi\kappa_w)^{-1/2}\alpha_2\lambda_w\exp(-\zeta^2)\}$$

with $\zeta = \alpha_4/\kappa_w^{1/2}$, $\eta = \alpha_4/\kappa_i^{1/2}$ and $\gamma = \alpha_4/D^{1/2}$.

For $T_A = -3°C$, $T_\infty = 1°C$ and $S_\infty = 10$, the numerical values are:

$$\alpha_1 = -19.62°C \quad \alpha_2 = 3.30°C$$

$$\alpha_3 = -78.88 \quad \alpha_4 = 6.48 \times 10^{-5}\ m\ s^{-1/2}.$$